Mitochondrial threshold for H2O2 release in skeletal muscle of mammals

Yann Voituron, Mélanie Boël, Damien Roussel

Mitochondrial threshold for H_2O_2 release in skeletal muscle of mammals

Voituron Yann*, Boël Mélanie and Roussel Damien

Université de Lyon, Université Claude Bernard Lyon 1, CNRS, ENTPE, UMR5023 LEHNA, F-69622, Villeurbanne, France

*To whom correspondence should be addressed: LEHNA, UMR 5023, CNRS, Université Claude Bernard Lyon 1, Bâtiment Charles Darwin C, F-69622 Villeurbanne Cedex, France
E-mail: yann.voituron@univ-lyon1.fr

Running title: A universal threshold for H_2O_2 release in mammals

Keywords: Allometry; Bioenergetics; Oxidative phosphorylation; Skeletal muscle; Radical oxygen species.

Abstract

The aim of the study was to evaluate the interplay between mitochondrial respiration and H_2O_2 release during the transition from basal non-phosphorylating to maximal phosphorylating states. We conducted a large scale comparative study of mitochondrial oxygen consumption, H_2O_2 release and electron leak (% H_2O_2/O) in skeletal muscle mitochondria isolated from mammal species ranging from 7 g to 500 kg. Mitochondrial fluxes were measured at different steady state rates in presence of pyruvate, malate, and succinate as respiratory substrates. Every species exhibited a burst of H_2O_2 release from skeletal muscle mitochondria at a low rate of oxidative phosphorylation, essentially once the activity of mitochondrial oxidative phosphorylation reached 26% of the maximal respiration. This threshold for ROS generation thus appears as a general characteristic of skeletal muscle mitochondria in mammals. These findings may have implications in situations promoting succinate accumulation within mitochondria, such as ischemia or hypoxia.

1. Introduction

In cells, ROS are continuously produced as a byproduct of the mitochondrial oxidative phosphorylation process and more generally of aerobic metabolism (Kowaltowski et al., 2009; Murphy, 2009). Because of its relationship with oxygen consumption, the link between ROS production and metabolic rate has been extensively studied especially in the light of the free radical theory of aging (Müller et al., 2007). Body mass dependence of respiration rates has been largely reported in muscle and liver mitochondria from mammals and birds (Drabkin, 1950; Porter and Brand, 1993; 1995; Brand et al., 2003; Boël et al., 2019). An allometry of mitochondrial oxidative activity is consistent with the lower activity and/or content of mitochondrial oxidative enzymes reported in several tissues of large mammals compared with small species (Drabkin, 1950; Fried and Tipton, 1953; Kunkel et al., 1956; Emmett and Hochachka, 1981; Phillips et al., 2012). Consequently, all studies found a negative correlation between the specific oxygen consumption and body mass at all levels of organization, from whole body to cell and mitochondria. However, regarding mitochondrial ROS production and body mass, similar pattern is often observed in different taxa (Sohal et al., 1989; 1990; Ku et al., 1993; Sohal and Weindruch, 1996; Csiszar et al., 2012; Roussel et al., 2015), but not systematically so (e.g. depending on the substrate used) (Lambert et al., 2007; Csiszar et al., 2012; Montgomery et al., 2012). One part of the discrepancies between studies could be explained by the fact that mitochondrial generation of ROS is a complex process which results in the sum of rates from up to eleven mitochondrial sites involved in substrate oxidation and electron transport (Brand, 2016).

Notwithstanding such a complex picture of mitochondrial ROS production, the main driver of ROS generation and electron leak (the ratio ROS/O) remains the reduction state of the electron donors in the mitochondrial electron transport system (Quinlan et al., 2013). It has been clearly shown that the ROS generation is non-linearly sensitive to the redox state of respiratory chain intermediates but also to the proton motive force value and so the energetic state of mitochondria (Korshunov et al., 1997; Votyakova and Reynolds, 2001; Starkov and Fiskum, 2003; Kikusato and Toyomizu, 2013; Cortassa et al., 2014; Quinlan et al., 2012; Goncalves et al., 2015; Treberg et al., 2018). For instance, when mitochondria increase their activity from basal respiration to maximal phosphorylating respiration, there is a 10% decrease in membrane potential but a 10 fold reduction in ROS generation (Korshunov et al., 1997; Starkov and Fiskum, 2003; Kikusato and Toyomizu, 2013). Thereby, ROS generation is maximal at the non-phosphorylating state when the high value of the proton motive force restricts the respiration rate and corresponding electron flux, leading to increased electron leak

and ROS formation (Treberg et al., 2018). In contrast, ROS generation decreases as the intensity of phosphorylating activity increases, reaching a minimum at maximal phosphorylating activity, due to a higher oxidized state of electron transporter intermediates (Starkov and Fiskum, 2003; Barja, 2007; Quinlan et al., 2012; Goncalves et al., 2015; Roussel et al., 2019).

So far, previous works on mitochondrial ROS production have essentially reported on basal non-phosphorylating and maximal phosphorylating states. Such double assessment is useful to compare species, populations or individuals facing environment variations but does not fully reflect the interplay between oxygen consumption and ROS formation particularly at intermediate activity levels. Indeed, mitochondria working in the cells are never in a basal non-phosphorylating state and are only rarely running ATP synthesis at full maximal capacity. ROS generation remains low until a threshold value of mitochondrial activity is reached, at which point this production abruptly increases (Roussel et al., 2019). For instance, mitochondrial oxidative phosphorylation activity of skeletal muscles in ducklings had to be reduced by 60-70% before mitochondrial ROS production sharply increased (Roussel et al., 2019). At some point, such a threshold value defines the frontier between two contrasted functional states of mitochondria: i) one state characterized by a high ATP production and a moderate ROS production, and ii) another state characterized by a low ATP production and a high ROS production.

On the whole, the variation of mitochondrial thresholds for H_2O_2 generation is globally unknown in animals. Therefore, the aim of the present study was to i) evaluate the interplay between mitochondrial respiration and H_2O_2 release or electron leak ($\%H_2O_2/O$) during the transition from basal non-phosphorylating (LEAK) to maximal oxidative phosphorylating (OXPHOS) states in different mammals' skeletal muscle mitochondria, ii) estimate the range of variation of the resulting threshold values, i.e. the mitochondrial activity level at which H_2O_2 release from mitochondria start to increase dramatically and iii) assess the allometry of these parameters in mammal species ranging from 7 g to 500 kg.

2. Materials and methods

2.1. Animals and tissue sampling

All experiments were conducted in accordance with animal care guidelines and were approved by the Ethics Committee of Lyon and the Ministère de la Recherche et de l'Enseignement Supérieur. All animals used in the present study were males. African pygmy mice (*Mus minutoides*) and house mice (*Mus musculus*) were obtained from laboratories

(respectively ISEM, Montpellier, France and LBBE, Lyon, France) and killed by cervical dislocation. Syrian hamsters (*Mesocricetus auratus*) and black rats (*Rattus rattus*) were obtained from laboratories (Chronobiotron, Strasbourg, France for *M. auratus*; Jardin Zoologique de la Citadelle, Besançon, France for *R. rattus*) and were killed under isoflurane-induced general anesthesia. Fresh tissues for bovines (*Bos taurus*) and sheep (*Ovis aries*) were obtained from a local slaughter house (Cibevial, Corbas, France). Fresh tissues for all other mammals were obtained from pest control (nutria - *Myocastor coypus* and muskrat - *Ondatra zibethicus*), local farmers (rabbits – *Oryctolagus cuniculus*) or Fondation Pierre Vérot at Saint-André-de-Corcy, France (boar – *Sus scrofa*).

2.2 Mitochondrial isolation

Fresh muscle tissue from every mammal studied was used for mitochondrial extraction. Mitochondria were isolated from the hind-limb muscles for the two smallest species (*M. minutoides* and *M. musculus*), from a mixture of gastrocnemius and quadriceps muscles for medium-size species (*M. auratus, R. rattus*, *M. coypus*, *O. zibethicus*, *O. cuniculus*), and from a sampling of the fore-leg muscles for the largest species (*O. aries*, *S. scrofa*, *B. taurus*). For pygmy mice, skeletal muscle samples from three individuals were used for each mitochondrial preparation. Muscle mitochondria were isolated in an ice-cold isolation buffer (100 mM sucrose, 50 mM KCl, 5 mM EDTA, 50 mM Tris-base, and pH 7.4). Briefly, the mitochondrial isolation procedure involved Potter homogenization, protease digestion and differential centrifugations, with all steps at 4°C as described previously (Boël et al., 2019). Finally, skeletal muscle mitochondrial populations were pelleted at 8,700×g (10 min) and the protein concentration of the mitochondrial suspension was determined by a Biuret method with bovine serum albumin as standard.

2.3 *Mitochondrial oxygen consumption rate*

Mitochondrial oxygen consumption rates were determined at 37°C in a respiratory buffer (120 mM KCl, 5 mM KH_2PO_4, 1 mM EGTA, 2 mM $MgCl_2$, 0.3% fatty acid-free bovine serum albumin, 1.6 U/mL hexokinase, 20 mM glucose, and 3 mM Hepes, pH 7.4). Mitochondria were energized by adding pyruvate/malate (5/2.5 mM) followed by 5 mM succinate and the rates of basal respiration recorded. Active phosphorylating respiration was initiated by the addition of 4, 10, 20, 100 and 500 µM ADP (Boël et al., 2019). The rate of oxygen consumption was recorded in a closed glass cell fitted with a Clark oxygen electrode (Rank Brothers Ltd, Cambridge, UK). Respiratory control ratio (RCR) was calculated as the ratio

between the rates of ADP (500 µM)-induced phosphorylating respiration to basal non-phosphorylating respiration.

2.4 Mitochondrial reactive oxygen species production

The rate of H_2O_2 released by isolated mitochondria was measured in the respiratory buffer at 37°C using a fluorometer (SFM-25, Kontron Instrument, Augsburg, Germany) at excitation and emission wavelengths of 560 nm and 584 nm, respectively. The respiratory buffer was supplemented with 5 U/mL horseradish peroxidase and 1 µM Amplex Red fluorescent dye. Respiratory substrates were successively added with 5 mM pyruvate/2.5 mM malate followed by 5 mM succinate and the rates of H_2O_2 generation recorded. Thereafter, H_2O_2 generation was titrated with the sequential addition of ADP at final concentrations of 4, 10, 20, 100, and 500 µM. The fluorescent signal was finally calibrated using a standard curve obtained after successive addition of H_2O_2 (up to 35 pmoles). Electron leak (%H_2O_2/O) was calculated as the fraction (%) of the total electron flow that reduces oxygen into H_2O_2 instead of reaching cytochrome-c oxidase to reduce oxygen into water (Rey et al., 2013).

2.5. Statistical analyses

The individual breakpoint values of oxygen consumption for significant H_2O_2 release have been determined using the package 'segmented' of R core Team. Subsequently, the threshold values for mitochondrial H_2O_2 release representing the percentage maximal oxidative phosphorylation rate at which H_2O_2 release started to increase sharply were determined individually. Following the determination of these parameters, all statistical analyses were conducted on data corrected by the Phylogenetic Independent Contrast model in order to get them phylogenetically independent. From the mammal phylogenetic super-tree proposed by Fritz et al. (2009), a phylogenetic tree with the ten species chosen in the present study was created. Thereafter, the data were corrected by the PIC function that applies the Phylogenetic Independent Contrast method described by Felsenstein (1985), assuming that the evolution model for life-history traits follows Brownian motion. After transforming body mass and H_2O_2 release by the common logarithm (log 10), the relationship between these two variables was analyzed with the linear model, with $\log_{10}$(body mass) as a fixed factor. The same statistical analyses were made to investigate the impact of body mass on oxygen consumption rate, electron leak, or threshold value. Fits were performed on $\log_{10}$-transformed data with the linear model, with $\log_{10}$(body mass) as fixed factor. For all these allometric relationships, normality and homoscedasticity criteria for the model's residues were checked by the

Shapiro-wilk normality test coupled to the Plot Diagnostics for a lm object. Statistical analyses were done with the R Core Team (R Core Team, 2018) and the packages 'phytools', 'ape', 'multcomp', 'mvtnorm', 'survival', 'TH.data', and 'MASS'.

3. Results

3.1. Mitochondrial bioenergetics parameters

In the present protocol, mitochondria were energized with pyruvate/malate and the resulting rates of oxygen consumption and H_2O_2 release were recorded before succinate was added in the respiratory chamber. The basal non-phosphorylating respiration rate of skeletal muscle mitochondria respiring on pyruvate/malate was significantly decreased with an increasing body mass of mammals ($F_{(1,8)} = 10.38$; $p < 0.05$; Fig. 1). In contrast, the rate of H_2O_2 release from mitochondria respiring on pyruvate/malate ($F_{(1,8)} = 2.55$; $p = 0.15$; Fig. 2) and the corresponding % H_2O_2/O ($2.30 \times mass^{0.013}$; $r^2 = 0.011$; $F_{(1,8)} = 0.23$; $p = 0.64$; data not shown) were not significantly related to body mass.

Table 1 describes several bioenergetics parameters of mitochondria isolated from the skeletal muscle of the ten mammalian species and respiring on pyruvate/malate/succinate in both basal and ADP-induced active phosphorylating state. The rates of mitochondrial oxygen consumption significantly decreased with increasing body mass in both the basal state ($J_O = 157 \times mass^{-0.12}$; $r^2 = 0.85$; $F_{(1,8)} = 13.94$, $p < 0.01$) and in the active state, i.e. at maximum rates of ATP synthesis ($J_O = 761 \times mass^{-0.10}$; $r^2 = 0.67$; $F_{(1,8)} = 7.77$, $p < 0.05$). The rate of H_2O_2 release was also related to body mass but only in the active state ($J_{H2O2} = 660 \times mass^{-0.091}$; $r^2 = 0.33$; $F_{(1,8)} = 6.38$, $p < 0.05$); the variation in the basal state failed to reach significance ($J_{H2O2} = 4786 \times mass^{-0.073}$; $r^2 = 0.50$; $F_{(1,8)} = 4.61$, $p = 0.06$). The electron leak (%ROS/O) was not correlated with body mass in either the basal or active states (%H_2O_2/O $= 3.06 \times mass^{0.048}$; $r^2 = 0.31$; $F_{(1,8)} = 0.11$; $p = 0.74$ and % H_2O_2/O $= 0.09 \times mass^{0.007}$; $r^2 = 0.003$; $F_{(1,8)} = 0.92$; $p = 0.37$, in basal and active states respectively).

3.2. Relationships between H_2O_2 generation and oxygen consumption

Mitochondrial H_2O_2 release and oxygen consumption at different mitochondrial phosphorylating steady-state rates are presented in Fig. 2. H_2O_2 generation and electron leak (%H_2O_2/O) decreased non-linearly as mitochondrial oxidative phosphorylation activity increased. From the maximum oxidative phosphorylation state to the basal state (from right to left in Fig 2), the rate of H_2O_2 release and corresponding % H_2O_2/O increased slowly at high

oxygen consumption, up to a phosphorylating steady-state rate below which a sharp increase in these parameters occurred. The rate of oxygen consumption at which H_2O_2 release start to increase sharply (i.e. the breaking point of the non-linear curve shown in Fig. 2) was determined for each individual of the ten mammal groups (see "Materials and Methods" section for more details). Fig. 3 shows that the oxygen consumption rate at the breakpoint is negatively correlated with body mass ($F_{(1,8)} = 30.87$; $p < 0.05$), but the correlation was not quite significant when data were corrected for phylogenetic relatedness of species ($F_{(1,8)} = 4.84$; $p = 0.059$).

3.3. Threshold values of mitochondrial ROS generation

The above result indicates that small mammals trigger a sharp H_2O_2 release at higher oxygen consumption rate than larger species. However, the respiratory activities of mitochondria from small mammals were also significantly higher than in larger species (Table 1). To test whether the higher mitochondrial oxidative activity of small mammals was responsible for the shift, we expressed the oxygen consumption rate at the inflexion point as a percentage of maximal oxidative rate. This fractional value defines a threshold in mitochondrial H_2O_2 release for each of the ten mammal species, i.e. the percentage maximal oxidative rate at which H_2O_2 release starts to increase sharply (Roussel et al., 2019). Fig. 3 indicates that threshold values were independent of body mass ($F_{(1,8)} = 0.0002$, $p = 0.99$). Regardless of the species studied, the oxidative phosphorylation activity had to decrease by approximately 74% before a major increase in H_2O_2 release occurred in skeletal muscle mitochondria.

4. Discussion

We followed the entire non-linear dynamic relationship between the intensity of oxidative phosphorylation (i.e. from basal non-phosphorylating to maximal phosphorylating rates) and mitochondrial H_2O_2 release or electron leak (%H_2O_2 /O) in ten mammal species. The present results show a clear threshold for mitochondrial H_2O_2 release and electron leak (%H_2O_2 /O), which remain low until a low level of oxidative phosphorylation activity is reached. Hence, the activity of mitochondrial oxidative phosphorylation must reach 26% of the maximal respiration before an H_2O_2 release burst occurs in skeletal muscle of mammals. The threshold values for H_2O_2 release in mammals are slightly lower than those recently published in birds (Roussel et al., 2019). Compared with the value of 26% in skeletal muscle mitochondria from mammals (present study), the threshold values for H_2O_2 release in skeletal muscle mitochondria from ducklings average 35% of the maximal oxidative phosphorylation activity,

ranging from 25% to 45% depending on nutritional status and muscle phenotypes (Roussel et al., 2019). It has been clearly shown that the ROS generation is non-linearly sensitive to the redox state of respiratory chain intermediates, which remain the main driver of ROS generation (Quinlan et al., 2013). Thus, the kinetics of ROS release could be well explained by the rate of electron leak to generate ROS, which decreases non-linearly during the transition from basal to maximal phosphorylating activity due to an enhanced oxidized state of electron transport chain intermediates (Quinlan et al., 2013; Starkov and Fiskum, 2003; Cortassa et al., 2014). These studies further suggest that the non-linear relationships between H_2O_2 release and mitochondrial activity might be a general feature of mammal and avian mitochondrial functioning, i.e. a low release of H_2O_2 followed by a sharp increase once a threshold of oxidative phosphorylation inactivity is reached.

Previous studies have reported a negative relationship between body mass and mitochondrial ROS production in several mammalian tissues, including kidney, heart and liver (Sohal et al., 1990; Ku et al., 1993; Lambert et al., 2007). The present data also show that the rates of H_2O_2 release during basal non-phosphorylating respiration and maximal phosphorylating respiration in skeletal muscle mitochondria respiring on pyruvate/malate/succinate were on the whole negatively correlated with body mass of mammals. Yet, mitochondrial respiration and H_2O_2 emission may vary according to the muscle phenotypes, being respectively high and low in slow twitch/oxidative muscle and conversely in fast twitch/glycolytic muscle (Anderson and Neufer, 2006; Picard et al., 2008). In the present study, we assumed that collected muscles were predominantly constituted of mixed glycolytic/oxidative muscle fibers and representative of the whole musculature across the ten species. Nevertheless, it has been reported that for a given skeletal muscle, the activities of oxidative and glycolytic enzymes negatively and positively correlate to body mass in mammals, respectively (Emmett and Hochachka, 1981). If the metabolic (oxidative/glycolytic) and contractile (slow/fast twitch) phenotypes are related each other across mammalian species, then we should expected the mitochondrial oxidative activity and H_2O_2 emission in small mammals to be respectively greater (which was the case in the present study) and lower (which was not the case in the present study) than in large mammals. Although, we cannot exclude differences in the composition of skeletal muscle fiber types between mammalian species, we suggest that this characteristic was not the main driver of the negative relationship between body mass and mitochondrial H_2O_2 release reported here.

Further insight, it is important to keep in mind that we did not directly measure mitochondrial ROS production, but the rate of H_2O_2 release from mitochondria, which is a

function of ROS producing and consuming processes within mitochondria. Allometry studies on mitochondrial antioxidant systems are scarce, but there is some data suggesting no strong relationship between antioxidant enzyme activities of different tissues and body mass in mammals (Tolmasoff et al., 1980; Sohal et al., 1990; Stuart et al., 2013), including mitochondrial superoxide dismutase (Page et al., 2010). Another study on four species (camel, goat, rat and mouse) suggests that the activity of mitochondrial glutathione peroxidase might be negatively related to body mass (Al-Otaiba et al., 2010). Although this result has to be confirm with a larger number of species, it would be associated with a higher H_2O_2 release from mitochondria of large mammals, which is not the case (present study) (Sohal et al., 1990; Ku et al., 1993; Lambert et al., 2007). If mitochondrial antioxidant systems were the main determinant, the rate of H_2O_2 release from mitochondria respiring on pyruvate/malate should be as significantly correlated with body mass as in the presence of succinate, which was not the case (present study). Even though, we cannot completely rule out the possible influence of interspecific differences in the matrix H_2O_2 consuming processes, these processes were not the main driver of the negative allometric relation reported in muscle mitochondria respiring on pyruvate/malate/succinate (Table 1).

Of note, these interspecific correlations between body mass and mitochondrial ROS release are essentially reported when mitochondria are respiring on succinate (Lambert et al., 2007). Succinate oxidation generates ROS production both with a reverse electron transfer at the quinol site of complex I and with a forward reaction at the flavin site of complex II (Quinlan et al., 2012b). Interestingly, these two sites account for half of the total rate of H_2O_2 production in skeletal muscle mitochondria during rest (Goncalves et al., 2015). In the present study, the addition of succinate in mitochondria respiring on pyruvate/malate resulted in a drastic increase in H_2O_2 release, which was highly sensitive to the addition of ADP (Table 1). Such high dependence of H_2O_2 release upon mitochondrial activity (basal non-phosphorylating state *versus* active phosphorylating state) suggests that the reverse electron transfer through complex I would be involved in the differences in the H_2O_2 release between species (Zoccaroto et al., 2009; Goncalves et al., 2015). Indeed, the endergonic nature of the reversed electron transport makes ROS generation by this process highly sensitive to proton motive force (Korshunov et al., 1997; Votyakova and Reynolds, 2001; Starkov and Fiskum, 2003), and so to proton motive force consuming pathways such as ATP synthesis. These observations thus suggest that the low level of H_2O_2 production in the larger mammals might result from a low content of complex I (Lambert et al., 2010). The allometry of ROS production in mammals might also be explained by changes in complex II level and/or

activity. This is suggested by an earlier study reporting a negative relationship between the activity of succinate oxidase and body mass in several tissues of mammals (Fried and Tipton, 1953). Nevertheless, the ROS generation from complex II reaches a maximum at a low concentration of succinate (<400 µM), becoming very low at high concentrations (Quinlan et al., 2012b), such as the 5 mM used in the present study. We thus postulate that the low level of H_2O_2 production in mitochondria from the larger mammals would result mainly from a lower activity of the reversed electron transport through complex I, a hypothesis that remains to be investigated thoroughly.

The quinol site in complex I, which is active during reverse electron transport, produces a significant rate of ROS in resting skeletal muscle, heart and cell lines from several other tissues (Goncalves et al., 2015; Brand et al., 2016; Wong et al., 2019). This ROS generation by the reverse electron transport in complex I is exacerbated with increasing concentrations of succinate (Zoccaroto et al., 2009). Hence, this mechanism appears to be of pathological and physiological importance in situations promoting succinate accumulation within mitochondria, such as ischemia or hypoxia (Hochachka et al., 1975; Starkov, 2008; Ralph et al., 2011). Succinate accumulates in several tissues of mammals, including heart, liver, kidney and brain during ischemia (Chouchani et al., 2013), or during breath-hold dives (Hochachka et al., 1975). During reperfusion, its rapid oxidation leads to a burst of ROS production and ischemia-reperfusion injury (Dröse, 2013; Chouchani et al., 2016). In turn, the ROS release from mitochondria could also serve as a signal, which may regulate cell functions (Guzy and Schumaker, 2006; Stowe and Camara, 2009). For instance, ROS play a vital role in the regulation of muscle metabolism and adaptation towards exercise (Morales-Alamo and Calbet, 2016). ROS signaling may also be involved in the up-regulation of antioxidant pathways and repair mechanisms of cellular damage reported in diving vertebrates, limiting the oxidative stress associated with repeated prolonged apnea and re-oxygenation cycles (Filho et al., 2002; Rey et al., 2016). Another interesting perspective is the differential oxygen sensitivity of these two mitochondrial processes, i.e. the oxygen respiration and the H_2O_2 release (Hoffman et al., 2007; Treberg et al., 2018). This oxygen sensitivity of mitochondrial ROS generation varies between the respiratory substrates and the ROS-generating sites within mitochondria (Hoffman and Brookes, 2009). For instance, it has been shown that complex I remains the main source of ROS generation at low concentration of oxygen (Hoffman and Brookes, 2009). Whether the oxygen sensitivity differs between tissues and across mammalian species remain an open question.

Acknowledgements. We thank Ashley Nord for reviewing the English manuscript. We warmly thank the 'Jardin Zoologique de la Citadelle' in Besançon, 'l'Office National de la Chasse et de la Faune Sauvage de l'Ain', the 'Institut des Sciences de l'Evolution' (UMR5554-CNRS) in Montpellier, the 'Departement d'Ecologie, Physiologie et Ethologie' (Institut Pluridisciplinaire Hubert Curien, UMR7178-CNRS) in Strasbourg and the 'Laboratoire de Biométrie et Biologie Evolutive' (UMR5558-CNRS) in Lyon for tissue sources.

Author contributions. Conception of the study and design of the work: D.R., Y.V.; acquisition and analysis: D.R., M.B., Y.V.; interpretation of data and validation: D.R., M.B., Y.V.

Competing interests. The authors declare that they have no competing financial interests.

Data Sharing. Data available on request from the corresponding authors.

References

Al-Otaiba A, John A, Al-Belooshi T, Raza H, 2010. Redox homeostasis and respiratory metabolism in camels (*Camelus dromedaries*): comparisons with domestic goats and laboratory rats and mice. *J. Comp. Biochem. B* **180**, 1121-1132.

Anderson EJ, Neufer PD, 2006. Type II skeletal myofibers possess unique properties that potentiate mitochondrial H_2O_2 generation. *Am. J. Physiol.* **290**, C844-C851.

Barja G, 2007. Mitochondrial oxygen consumption and reactive oxygen species production are independently modulated: implications for aging studies. *Rejuven. Res.* **10**, 215-223.

Boël M, Romestaing C, Voituron Y, Roussel D, 2019. Allometry of mitochondrial efficiency is set by metabolic intensity. *Proc. R. Soc. B* **286**, 20191693.

Brand MD, 2016. Mitochondrial generation of superoxide and hydrogen peroxide as the source of mitochondrial redox signaling. *Free Rad. Biol. Med.* **100**, 14-31.

Brand MD, Turner N, Ocloo A, Else PL, Hulbert AJ, 2003. Proton conductance and fatty acyl composition of liver mitochondria correlates with body mass in birds. *Biochem. J.* **376**, 741-748.

Brand MD, Goncalves RLS, Orr AL, Vargas L, Gerencser AA, Jensen MB, Wang YT, Melov S, Turk CN, Matzen JT, *et al*., 2016. Suppressors of superoxide-H2O2 production at site IQ of mitochondrial complex I protect against stem cell hyperplasia and ischemia-reperfusion injury. *Cell Metab.* **24**, 582-592.

Chouchani ET, Pell VR, Gaude E, Aksentijević D, Sundier SY, Robb EL, Logan A, Nadtochiy SM, Ord ENJ, Smith AC, *et al*., 2013. Ischaemic accumulation of succinate controls reperfusion injury through mitochondrial ROS. *Nature* **515**, 431-435.

Chouchani ET, Pell VR, James AM, Work LM, Saeb-Parsy K, Frezza C, Krieg T, Murphy MP, 2016. A unifying mechanism for mitochondrial superoxide production during ischemia-reperfusion injury. *Cell Metab.* **23**, 254-263.

Cortassa S, O'Rourke B, Aon MA, 2014. Redox-optimized ROS balance and the relationship between mitochondrial respiration and ROS. *Biochim. Biophys. Acta* **1837**, 87-295.

Csiszar A, Podlutsky A, Podlutskaya N, Sonntag WE, Merlin SZ, Philipp EER, Doyle K, Davila A, Recchia FA, Ballabh P, *et al.*, 2012. Testing the oxidative stress hypothesis of aging in primate fibroblasts: is there a correlation between species longevity and cellular ROS production? *J. Gerontol. A* **67**, 841-852.

Drabkin DL, 1950. The distribution of the chromoproteins, hemoglobin, myoglobin, and cytochrome c, in the tissues of different species, and the relationship of the total content of each chromoprotein to body mass. *J. Biol. Chem.* **182**, 317-334.

399 Dröse S, 2013. Differential effects of complex II on mitochondrial ROS production and their
400 relation to cardioprotective pre- and postconditioning. *Biochim. Biophys. Acta* **1827**,
401 578-587.
402 Emmett B, Hochachka PW, 1981. Scaling of oxidative and glycolytic enzymes in mammals.
403 *Resp. Physiol.* **45**, 261-272.
404 Felsenstein J, 1985. Phylogenies and the comparative method. *Am. Nat.* **125**, 1-15.
405 Filho DW, Sell F, Ribeiro L, Ghislandi M, Carrasquedo F, Fraga CG, Wallauer JP, Simoes-
406 Lopes PC, Uhart MM, 2002. Comparison between the antioxidant status of terrestrial
407 and diving mammals. *Comp. Biochem. Physiol.* **133A**, 885-892.
408 Fried GH, Tipton SR, 1953. Comparison of respiratory enzyme levels in tissues of mammals
409 of different sizes. *Proc. Soc. Exp. Biol. Med.* **82**, 531-532.
410 Fritz SA, Bininda-Emonds ORP, Purvis A, 2009. Geographical variation in predictors of
411 mammalian extinction risk: big is bad, but only in the tropics. *Ecol. Lett.* **12**, 538-549.
412 Goncalves RLS, Quinlan CL, Perevoshchikova IV, Hey-Mogensen M, Brand MD, 2015. Sites
413 of superoxide and hydrogen peroxide production by muscle mitochondria assessed *ex*
414 *vivo* under conditions mimicking rest and exercise. *J. Biol. Chem.* **290**, 209-277.
415 Guzy RD, Schumaker PT, 2006. Oxygen sensing by mitochondria at complex III: the paradox
416 of increased reactive oxygen species during hypoxia. *Exp. Physiol.* **91**, 807-819.
417 Hochachka PW, Owen TG, Allen JF, Whittow GC, 1975. Multiple end products of
418 anaerobiosis in diving vertebrates. *Comp. Biochem. Physiol.* **50B**, 17-22.
419 Hoffman DL, Salter JD, Brookes PS, 2007. Response of mitochondrial reactive oxygen
420 species generation to steady-state oxygen tension: implications for hypoxic cell
421 signaling. *Am. J. Physiol.* **292**, H101-H108.
422 Hoffman DL, Brookes PS, 2009. Oxygen sensitivity of mitochondrial reactive oxygen species
423 generation depends on metabolic conditions. *J. Biol. Chem.* **284**, 16236-16245.
424 Kikusato M, Toyomizu M, 2013. Crucial role of membrane potential in heat stress-induced
425 overproduction of reactive oxygen species in avian skeletal muscle mitochondria. *PLoS*
426 *ONE* **8**, e64412.
427 Korshunov SS, Skulachev VP, Starkov AA, 1997. High protonic potential actuates a
428 mechanism of production of reactive oxygen species in mitochondria. *FEBS Lett.* **416**,
429 15-18.
430 Kowaltowski AJ, de Souza-Pinto NC, Castilho RF, A.E.Vercesi AE, 2009. Mitochondria and
431 reactive oxygen species. *Free Rad. Biol. Med.* **47**, 333-343.

Ku HH, Brunk UT, Sohal RS, 1993. Relationship between mitochondrial superoxide and hydrogen peroxide production and longevity of mammalian species. *Free Rad. Biol. Med.* **15**, 621-627.

Kunkel HO, Spalding JF, De Franciscis G, Futrell MF, 1956. Cytochrome oxidase activity and body weight in rats and in three species of large animals. *Am. J. Physiol.* **186**, 203-206.

Lambert AJ, Boysen HM, Buckingham JA, Yang T, Podlutsky A, Austad SN, Kunz TH, Buffenstein R, Brand MD, 2007. Low rates of hydrogen peroxide production by isolated heart mitochondria associate with long maximum lifespan in vertebrate homeotherms. *Aging Cell* **6**, 607-618.

Lambert AJ, Buckingham JA, Boysen HM, Brand MD, 2010. Low complex I content explains the low hydrogen peroxide production rate of heart mitochondria from the long-lived pigeon, *Columba livia*. *Aging Cell* **9**, 78-91.

Montgomery MD, Hulbert AJ, Buttemer WA, 2012. Does the oxidative stress theory of aging explain longevity differences in birds? I. Mitochondrial ROS production. *Exp. Gerontol.* **47**, 203-210.

Morales-Alamo D, Calbet JAL, 2016. AMPK signaling in skeletal muscle during exercise: Role of reactive oxygen and nitrogen species. *Free Rad. Biol. Med.* **98**, 68-77.

Muller FL, Lustgarten MS, Jang Y, Richardson A, Van Remmen H, 2007. Trends in oxidative aging theories. *Free Rad. Biol. Med.* **43**, 477-503.

Murphy MP, 2009. How mitochondria produce reactive oxygen species. *Biochem. J.* **417**, 1-13.

Page MM, Richardson J, Wiens BE, Tiedtke E, Peters CW, Faure PA, Burness G, Stuart JA, 2010. Antioxidant enzyme activities are not broadly correlated with longevity in 14 vertebrate endotherm species. *Age* **32**, 255-270.

Picard M, Csukly K, Robillard ME, Godin R, Ascah A, Bourcier-Lucas C, Burelle Y, 2008. Resistance to Ca^{2+}-induced opening of the permeability transition pore differs in mitochondria from glycolytic and oxidative muscles. *Am. J. Physiol.* **295**, R659-R668.

Porter RK, Brand MD, 1993. Body mass dependence of H^+ leak in mitochondria and its relevance to metabolic rate. *Nature* **362**, 628-630.

Porter RK, Brand MD, 1995. Causes of differences in respiration rate of hepatocytes from mammals of different body mass. *Am. J. Physiol.* **269**, R1213-R1224.

Quinlan CL, Treberg JR, Perevoshchikova IV, Orr AL, Brand MD, 2012a. Native rates of superoxide production from multiple sites in isolated mitochondria measured using endogenous reporters. *Free Rad. Biol. Med.* **53**, 1807-1817.

Quinlan CL, Orr AL, Perevoshchlkova IV, Treberg JR, Ackrell BA, Brand MD, 2012b. Mitochondrial complex II can generate reactive oxygen species at high rates in both the forward and reverse reactions. *J. Biol. Chem.* **287**, 27255-27264.

Quinlan CL, Perevoshchikova IV, Hey-Mogensen M, Orr AL, Brand MD, 2013. Sites of active oxygen species generation by mitochondria oxidizing different substrates. *Redox Biol.* **1**, 304-312.

Ralph SJ, Moreno-Sanchez R, Neuzil J, Rodriguez-Enriquez S, 2011. Inhibitors of succinate: quinone reductase/Complex II regulate production of mitochondrial reactive oxygen species and protect normal cells from ischemic damage but induce specific cancer cell death. *Pharm. Res.* **28**, 2695-2730.

Rey B, Roussel D, Rouanet JL, Duchamp C, 2013. Differential effects of thyroid status on regional H2O2 production in slow- and fast-twitch muscle of ducklings. *J. Comp. Physiol. B* **183**, 135-143.

Rey B, Dégletagne C, Bodennec J, Monternier PA, Mortz M, Roussel D, Romestaing C, Rouanet JL, Tornos J, Duchamp C, 2016. Hormetic response triggers multifaceted anti-oxidant strategies in immature king penguins (*Aptenodytes patagonicus*). *Free Rad. Biol. Med.* **97**, 577-587.

Roussel D, Salin K, Dumet A, Romestaing C, Rey B, Voituron Y, 2015. Oxidative phosphorylation efficiency, proton conductance and reactive oxygen species production of liver mitochondria correlates with body mass in frogs. *J. Exp. Biol.* **218**, 3222-3228.

Roussel D, Boël M, Mortz M, Romestaing C, Duchamp C, Voituron Y, 2019. Threshold effect in the H_2O_2 production of skeletal muscle mitochondria during fasting and refeeding. *J. Exp. Biol.* **222**, jeb196188.

Sohal RS, Svensson I, Sohal BH, Brunk UT, 1989. Superoxide anion radical production in different animal species. *Mech. Ageing Dev.* **49**, 129-135.

Sohal RS, Svensson I, Brunk UT, 1990. Hydrogen peroxide production by liver mitochondria in different species. *Mech. Ageing Dev.* **53**, 209-215.

Sohal RS, Weindruch R, 1996. Oxidative stress, caloric restriction, and aging. *Science* **273**, 59-63.

Starkov AA, Fiskum G, 2003. Regulation of brain mitochondrial H_2O_2 production by membrane potential and NAD(P)H redox state. *J. Neurochem.* **86**, 1101-1107.

Starkov AA, 2008. The role of mitochondria in reactive oxygen species metabolism and signaling. *Ann. N.Y. Acad. Sci.* **1147**, 37-52.

Stowe DF, Camara AKS, 2009. Mitochondrial reactive oxygen species production in excitable cells: modulators of mitochondrial and cell function. *Antiox. Red. Signal.* **11**, 1373-1414.

Stuart JA, Liang P, Luo X, Page MM, Gallagher EJ, Christoff CA, Robb EL, 2013. A comparative cellular and molecular biology of longevity database. *Age* **35**, 1937-1947.

Tolmasoff JM, Ono T, Cutler RG, 1980. Superoxide dismutase: correlation with life-span and specific metabolic rate in primate species. *Proc. Natl. Acad. Sci. USA* **77**, 2777-2781.

Treberg JR, Braun K, Zacharias P, Kroeker K, 2018. Multidimensional mitochondrial energetics: application to the study of electron leak and hydrogen peroxide metabolism. *Comp. Biochem. Physiol. B* **224**, 121-128.

Votyakova TV, Reynolds IJ, 2001. $\Delta\Psi_m$-dependent and –independent production of reactive oxygen species by rat brain mitochondria. *J. Neurochem.* **79**, 266-277.

Wong HS, Benoit B, Brand MD, 2019. Mitochondrial and cytosolic sources of hydrogen peroxide in resting C2C12 myoblasts. *Free Rad. Biol. Med.* **130**, 140-150.

Zoccaroto F, Cavallini L, Alexandre A, 2009. Succinate is the controller of O_2^-/H2O2 release at mitochondrial complex I: negative modulation by malate, positive by cyanide. *J. Bioenerg. Biomembr.* **41**, 387-393.

518 **Table 1: Properties of muscle mitochondria isolated from mammals of different mass.**

Species (n)	Body weight (g)	Respiration rate (nmol O.min^{-1}.mg protein^{-1})		H_2O_2 release (pmol H_2O_2.min^{-1}.mg protein^{-1})		Electron leak (%H_2O_2/O)	
		Basal state	Active state	Basal state	Active state	Basal state	Active state
Pygmy mouse (10) (*M. minutoides*)	7.2 ± 0.4	141 ± 8	832 ± 49	5,062 ± 357	1,035 ± 76	3.69 ± 0.32	0.13 ± 0.02
House mouse (5) (*M. musculus*)	18.8 ± 0.6	98 ± 4	518 ± 16	4,598 ± 728	643 ± 178	4.75 ± 0.86	0.12 ± 0.03
Golden hamster (8) (*M. auratus*)	105.5 ± 2.6	95 ± 6	418 ± 14	4,067 ± 290	483 ± 24	4.29 ± 0.17	0.12 ± 0.01
Black rat (8) (*R. rattus*)	194.4 ± 7.2	88 ± 10	487 ± 50	2,452 ± 212	216 ± 34	2.92 ± 0.27	0.04 ± 0.00
Muskrat (1) (*O. zibethicus*)	1,600	85	443	2,091	206	2.5	0.05
Rabbit (6) (*O. cuniculus*)	3,200 ± 301	43 ± 3	218 ± 9	2,041 ± 190	209 ± 27	4.84 ± 0.49	0.10 ± 0.01
Nutria (3) (*M. coypus*)	5,150 ± 760	51 ± 2	222 ± 25	2,254 ± 418	181 ± 30	4.42 ± 0.83	0.08 ± 0.01
Sheep (6) (*O. aries*)	34,217 ± 1,633	42 ± 7	334 ± 60	1,834 ± 173	311 ± 92	4.97 ± 0.70	0.08 ± 0.01
Boar (5) (*S. scrofa*)	79,800 ± 4,420	52 ± 7	211 ± 18	3,422 ± 357	460 ± 36	6.94 ± 0.80	0.23 ± 0.03
Bovine (4) (*B. Taurus*)	486,300 ± 25,367	36 ± 5	260 ± 39	2,112 ± 226	242 ± 63	6.21 ± 0.85	0.09 ± 0.01

519 Values are means ± SEM [number of independent mitochondrial preparations (n) in parentheses alongside the name of animals]. Basal state of
520 respiration was initiated by the addition of pyruvate/malate/succinate (5/2.5/5 mM) as respiratory substrates. Active state of respiration was
521 measured following the addition of 500 µM ADP

Figure legends

Figure 1: Body mass dependence of basal respiration rate (J_O) and H_2O_2 release (J_{H2O2}) in skeletal muscle mitochondria respiring on pyruvate/malate. Skeletal muscle mitochondria were isolated from ten mammal species. Red symbols are two species taken to cover the whole range of body mass (bovine with the highest mass and pygmy mice with the lowest mass). Values are mean ± s.d. from (n) independent mitochondrial preparations; (n) is given alongside the name of the species

Figure 2: Relationships between oxidative phosphorylation activity and H_2O_2 release (A) or electron leak (B). Mitochondria were isolated from skeletal muscle of ten mammal species and were respiring on pyruvate/malate/succinate. Red symbols illustrate the relationships for two species taken to cover the whole range of body mass (bovine with the highest mass and pygmy mice with the lowest mass). Values are mean ± s.d. from (n) independent mitochondrial preparations; (n) is given alongside the name of the species

Figure 3: Body mass dependence of threshold H_2O_2 production values. Data are expressed as the oxygen consumption rate at the breaking point of H_2O_2 release or as a percentage of maximal oxidative phosphorylation activity (see text for more details) in skeletal muscle mitochondria isolated from ten mammal species. A mixture of pyruvate/malate/succinate was used as respiratory substrates. Red symbols are two species taken to cover the whole range of body mass (bovine with the highest mass and pygmy mice with the lowest mass). Values are mean ± s.d. from (n) independent mitochondrial preparations; (n) is given in Fig. 2 alongside the name of the species.

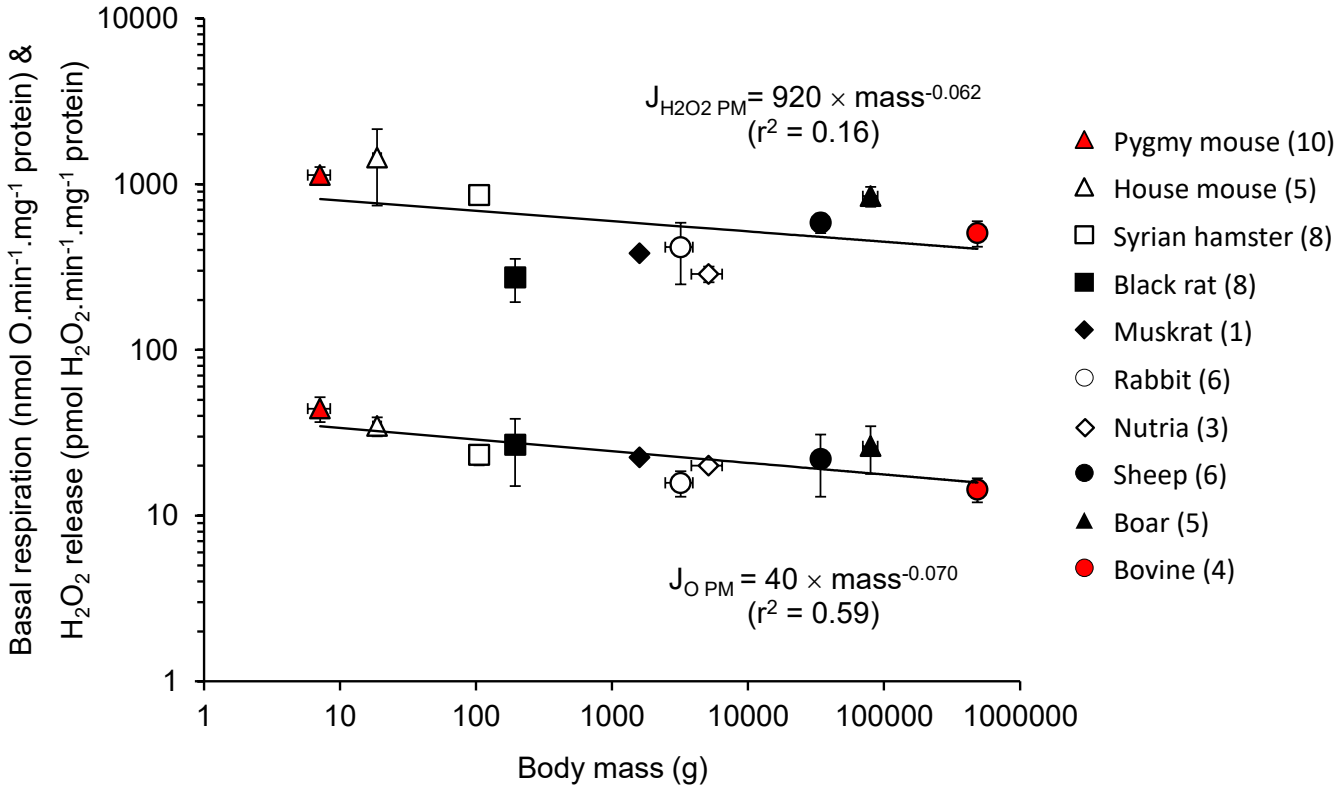
Basal respiration (nmol O.min-1.mg-1 protein) &
H2O2 release (pmol H2O2.min-1.mg-1 protein)
10000
1000
100
10
1
1
10
100
1000
10000
100000
1000000
Body mass (g)
JH2O2 PM= 920 × mass-0.062
(r2 = 0.16)
JO PM = 40 × mass-0.070
(r2 = 0.59)
Pygmy mouse (10)
House mouse (5)
Syrian hamster (8)
Black rat (8)
Muskrat (1)
Rabbit (6)
Nutria (3)
Sheep (6)
Boar (5)
Bovine (4)

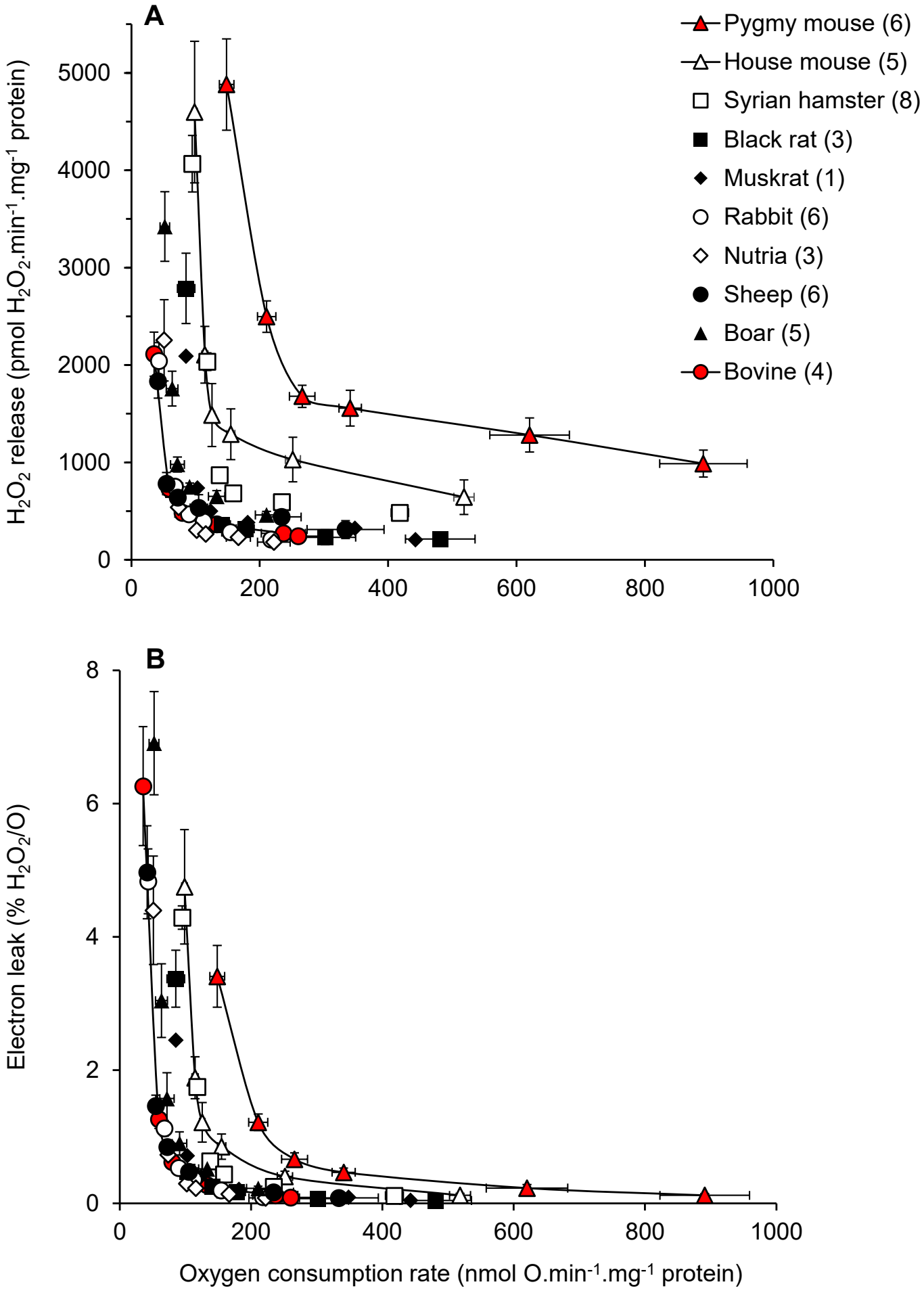
A
B
Pygmy mouse (6)
House mouse (5)
Syrian hamster (8)
Black rat (3)
Muskrat (1)
Rabbit (6)
Nutria (3)
Sheep (6)
Boar (5)
Bovine (4)
H2O2 release (pmol H2O2.min-1.mg-1 protein)
Electron leak (% H2O2/O)
Oxygen consumption rate (nmol O.min-1.mg-1 protein)
0
1000
2000
3000
4000
5000
0
200
400
600
800
1000
2
4
6
8

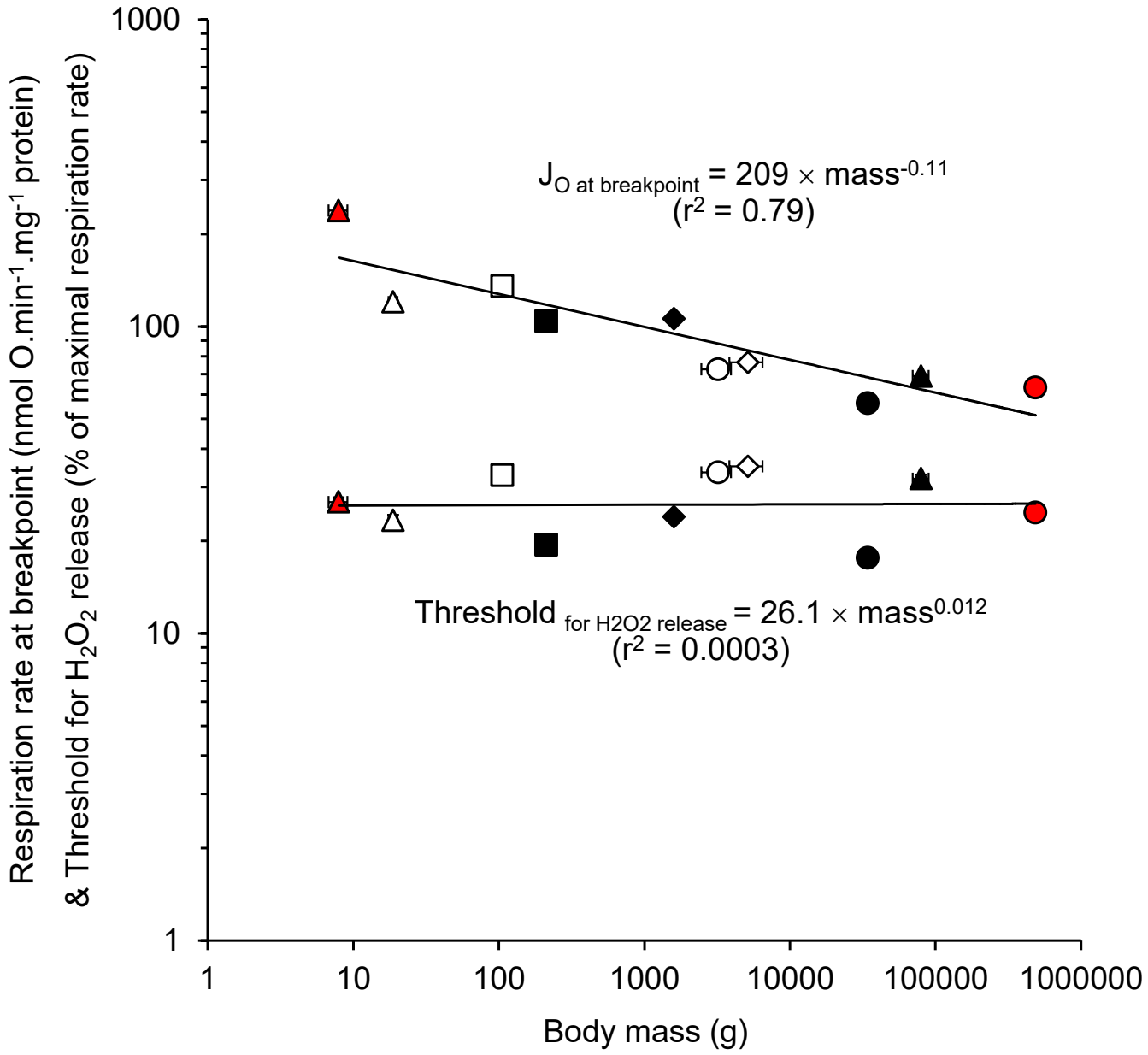
1000
100
10
1
1
10
100
1000
10000
100000
1000000
Body mass (g)
Respiration rate at breakpoint (nmol O.min-1.mg-1 protein)
& Threshold for H2O2 release (% of maximal respiration rate)
JO at breakpoint = 209 × mass-0.11
(r2 = 0.79)
Threshold for H2O2 release = 26.1 × mass0.012
(r2 = 0.0003)